JOURNAL OF MATERIALS SCIENCE 23 (1988) 1206–1218

Precipitation and irradiation damage in proton-irradiated palladium–chromium alloys

J. C. HUANG, A. J. ARDELL, O. AJAJA*
Department of Materials Science and Engineering, University of California, Los Angeles, California 90024, USA

Irradiation damage of Pd–Cr alloys containing 15, 20 and 25 at% Cr was studied over the temperature range 100 to 550° C, primarily in samples irradiated to a dose of 0.7 d.p.a. The solubility limit in this range of temperatures varies from 22 to 38% Cr, and precipitation of a phase having the $L1_2$ crystal structure was observed in unirradiated samples of the 25% Cr alloy aged at temperatures as low as 100° C. Octahedrally shaped voids, with faces parallel to $\{1\,1\,1\}$, were found only in the 25% Cr alloy irradiated from 350 to 550° C, but not in the other alloys at any temperature. The undersized chromium atoms migrate to point-defect sinks during irradiation, resulting in solute segregation and, eventually, precipitation under certain conditions. The precipitation of the $L1_2$ phase, which is the thermodynamically stable phase at higher chromium contents, was irradiation-induced at dislocation loops, voids and grain boundaries in the more concentrated undersaturated alloys. This irradiation-induced precipitation was observed in the mid-range and surface regions of the samples containing 20 and 25% Cr, but not in those containing 15% Cr. The behaviour of these alloys is compared with Pd–Fe and Ni–Si alloys, which have also been proton-irradiated in this laboratory, and the similarities and differences are noted and discussed.

1. Introduction

The radiation damage to which binary nickel-base alloys are subjected when bombarded by energetic particles has been studied extensively by numerous investigators (e.g. [1–5]). In addition to the usual damage produced by fast neutrons, heavy ions, high-voltage electrons and protons, e.g. voids and interstitial dislocation loops, the phenomena of irradiation-induced solute segregation (IISS) and irradition-induced precipitation (IIP) are commonly observed in Ni–Be [1] and especially Ni–Si alloys [2–4]. It had generally been taken for granted that Ni–Si and Ni–Be alloys were susceptible to IISS and IIP because the beryllium and silicon solutes are undersized atoms, and therefore preferentially occupy interstitial positions during irradiation. The biased diffusion of interstitials towards interstitial sinks thus induces a build-up of solute atoms at the sinks (IISS), which can lead to precipitation of a phase if the solute content exceeds the solubility limit (IIP).

The occurrence of IISS and IIP is associated with a parameter η, defined by the relationship $\eta = \mathrm{d}(\ln a)/\mathrm{d}c$, where a is the lattice constant and c is the solute concentration in atom fraction. In Ni–Be and Ni–Si alloys (in which IISS and IIP have been observed) $\eta < 0$, although IIP has also been seen in Ni–Ge alloys [5], where $\eta > 0$. It therefore seems that a negative value of η is not a prerequisite for the occurrence of IIP, but this cannot be determined solely on the basis of results on nickel-base alloys. This is partly due to the small size of the nickel atom, which severely limits the number of binary alloys containing undersized solutes that can be prepared. On the other hand, palladium is more ideally suited to a critical investigation of the role of η because its atomic size is intermediate among f c c metals and it is able to dissolve relatively large concentrations of numerous undersized as well as oversized solute atoms. In addition, palladium belongs to the same group as nickel in the periodic table and has a melting point only about 100° C higher than nickel. It is therefore reasonable to expect some similarities between the radiation damage behaviour of palladium and nickel. It was for these reasons that an experimental programme on the proton irradiation of palladium-base alloys was undertaken.

Some of the results of the proton-irradiation experiments on binary palladium-base alloys, particularly Pd–Fe [6], Pd–W [7, 8] and Pd–Mo [9] alloys, have already been compared with the findings of earlier work on nickel-base alloys [10, 11]. Among these alloys, only Pd–Fe alloys ($\eta = -0.0395$) exhibit behaviour remotely similar to that observed in Ni–Si alloys. For example, IIP of a phase with the Cu_3Au ($L1_2$) crystal structure is induced in both alloys under certain combinations of alloy concentration and irradiation temperature. However, two important characteristic phenomena, namely irradiation-induced homogeneous precipitation (IIHP) and surface films of Pd_3Fe (the counterpart of Ni_3Si) were never

Present address: Department of Physics, University of Ife, Ile-Ife, Nigeria.

0022–2461/88 $03.00 + .12

observed. This was attributed to the lower efficiency of iron atom transport by interstitial-iron atom coupling (compared to that in Ni–Si alloys) and to the rapid back-diffusion of iron atoms, which smooth the concentration gradients produced by the spatially inhomogeneous production of point defects within the proton range.

The present investigation was undertaken to determine whether the results of the study on Pd–Fe alloys were representative of the class of alloys expected to behave in a manner comparable to proton-irradiated Ni–Si alloys, i.e. whether the phenomena characteristically observed in Ni–Si alloys would generally be present or absent in palladium-base alloys irradiated under similar conditions. The Pd–Cr alloy system was selected for study because it has two important features in common with Pd–Fe and Ni–Si alloys: (i) at low temperatures the palladium-rich solid solution is in equilibrium with a phase which has the $L1_2$ crystal structure, and (ii) chromium is an undersized solute in palladium with $\eta = -0.025$ [10, 11], which is exactly the same as the value for silicon in nickel-base alloys.

2. Experimental procedures

The choice of alloy composition and irradiation temperature T_{irr}, was based on the phase diagram [12] shown in Fig. 1. The phase equilibria in this alloy system have not been studied extensively, so that Fig. 1 must be viewed with a degree of caution. The solubility limits, in particular, are uncertain and are therefore shown as dashed lines. Below 505° C the Pd–Cr solid solution is in equilibrium with a phase having the $L1_2$ crystal structure, the two-phase region existing within rather narrow composition limits. Between 505 and 570° C the solid solution is in equilibrium with a phase having the ordered $L1_0$ crystal structure. Since IIP was observed only in relatively concentrated Pd–Fe alloys (18 at % Fe), only concentrated alloys containing 15, 20 and 25 at % Cr

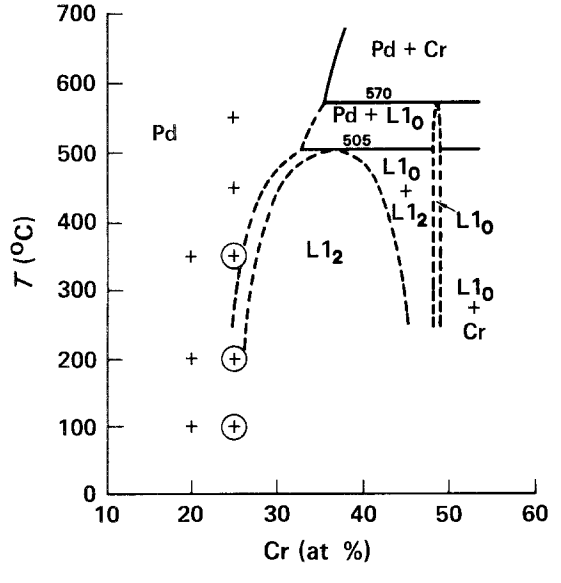

Figure 1 The palladium-rich region of the Pd–Cr phase diagram according to Raub *et al.* [12]. The ageing conditions are indicated by the plus signs, and those circled represent conditions in which the $L1_2$ phase was found after isothermal ageing of the unirradiated samples.

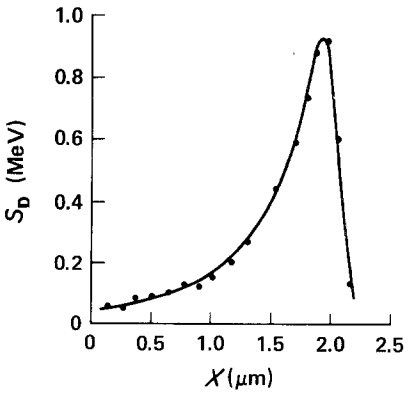

Figure 2 Damage energy profile expressed as the nuclear damage energy S_D against the distance X from the irradiated surface for 400 keV protons incident on a pure palladium target.

were prepared for this investigation. The alloys were prepared from high-purity starting materials (99.99% Pd, with 74 p.p.m. Pt as the major impurity, and 99.999% Cr) by induction melting. The alloys were remelted three times to ensure homogeneity and then reweighed. The weight losses were found to be less than 0.1% and therefore considered negligible. The ingots were then cold-rolled to sheet 0.11 to 0.14 mm in thickness. Discs 3 mm in diameter were then punched from the sheet and annealed at 1000° C in a vacuum, yielding homogeneous alloys of grain size 10 to 40 μm.

Prior to irradiation the disc samples were ground to a thickness of 0.1 to 0.12 mm using 4/0 emery paper and then electropolished using a jet-electropolishing apparatus. The electrolyte used was 90% acetic acid and 10% perchloric acid maintained at room temperature; this same electrolyte was also used for the preparation of thin foils of the irradiated samples examined in the transmission electron microscope (TEM), a Jeol 100CX Temscan operating at 100 keV. The samples were prepared for TEM after irradiation using the technique described previously [13]. The polishing rates were determined by an X-ray absorption method [14] using calculated values of the mass absorption coefficients of the alloys and employing freshly prepared electrolyte. The polishing rates for the three alloys were 446, 405 and 390 nm sec^{-1} for the 15, 20 and 25% Cr alloys, respectively. After irradiation the samples were jet-electropolished for a predetermined length of time at the surface which had been exposed to the proton beam. The sample was then inverted in the apparatus and polishing was continued until perforation occurred. It is possible using this method to examine the microstructure of an irradiated sample at a particular location within the proton range with an accuracy of ± 90 nm.

The damage profile for 400 keV protons incident on pure palladium is shown in Fig. 2. This profile was calculated using the TRIM code [15] and was used in all the calculations of the irradiation dose without correcting for the effect of chromium in solid solution. Comparison of the damage profiles for 400 keV protons incident on pure nickel and pure palladium [6] suggests that the effect of dissolved chromium on the defect production rate in the mid-range region is small. The dose displacements per atom (d.p.a.) was

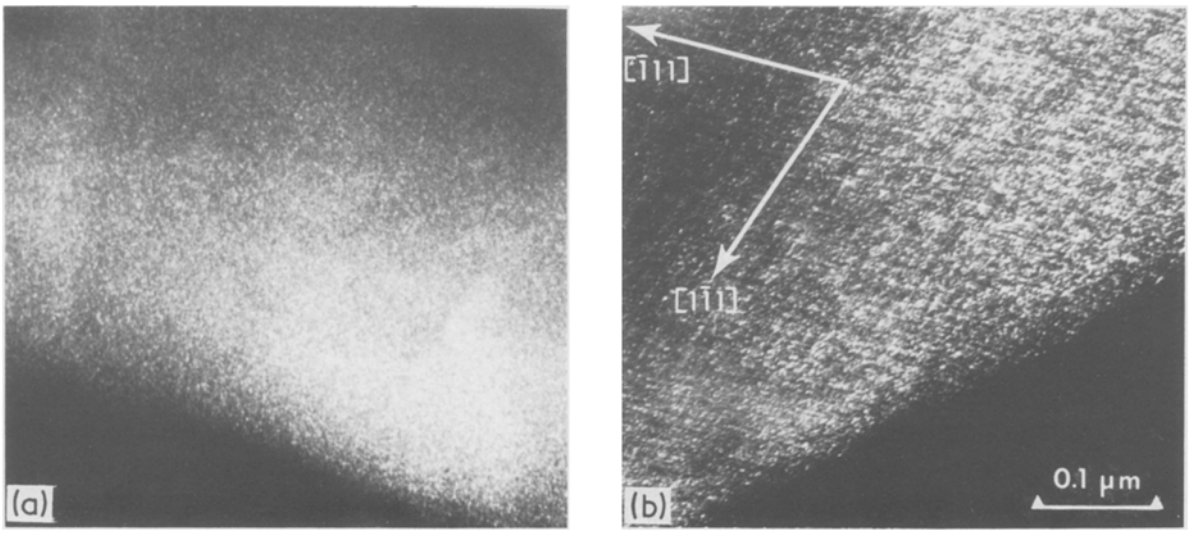

Figure 3 Dark-field electron micrographs, taken using superlattice reflections from the $L1_2$ phase, illustrating the effects of ageing the unirradiated 25% Cr samples at (a) 100° C for 7 days; (b) 350° C for 5 days. The foil orientation in (b) is [1 1 0], and the $\langle 1\,\bar{1}\,1 \rangle$ directions are indicated.

calculated from the formula [16]

$$\text{d.p.a.} = 0.8 S_D \phi t / 2 E_D n N_0 \delta \qquad (1)$$

where S_D is the damage energy for slabs of thickness δ and n ion histories (Fig. 2), ϕ is the proton flux, t is the irradiation time, E_D is the threshold displacement energy and N_0 is the number of target atoms per unit volume. In our experiments the current density was $0.195\,\mu A\,mm^{-2}$, $t = 1.08 \times 10^4$ sec, $n = 5000$, $\delta = 100$ nm and E_D was assumed equal to 40 eV. The dose and dose rate at a distance of 1.2 μm from the irradiated surface were calculated from Equation 1 to be 0.70 d.p.a. and 6.5×10^{-5} d.p.a. sec^{-1}, respectively. T_{irr} was varied over the range 100 to 550° C.

3. Results

3.1. Annealing experiments

In order to determine the phases present in the three alloys from 100 to 550° C a series of annealing experiments was undertaken. The 3 mm diameter samples were aged in a vacuum at various temperatures for 3 to 7 days and air-cooled to room temperature. Thin foils were then examined in the TEM to see if the electron diffraction patterns showed any evidence of the presence of another phase. The results of these experiments are summarized in Table I. No evidence of precipitation was found in the 15 to 20% Cr samples at any ageing temperature, but superlattice reflections belonging to a phase having the $L1_2$ crystal structure were observed in the 25% Cr samples at temperatures below 450° C. It is tempting to assign this phase the stoichiometry Pd_3Cr, which is typical of phases with this crystal structure. However, direct measurement of its composition was not possible, so this phase will henceforth be referred to as the $L1_2$ phase.

TABLE I Conditions for observation of the $L1_2$ phase in isothermally aged Pd–Cr alloys*

T (° C)	Ageing time (days)	Chromium concentration (at %)	
		20	25
100	7	N	Y
200	7	N	Y
350	5	N	Y
450	3	–	N
550	3	–	N

*Y = observed, N = not observed, (–) condition not studied.

At both 100 and 350° C the spatial distribution of the $L1_2$ phase was homogeneous, as seen in Fig. 3. It appears as if the precipitates are aligned along $\{1\,1\,1\}$ in the sample aged at 350° C (Fig. 3b), but no additional experiments were done to confirm this. The nucleation and growth of the equilibrium phase at an ageing temperature as low as 100° C in an alloy that melts above 1500° C seems rather remarkable, but this result was quite reproducible. The phase diagram in Fig. 1 also includes the results of the ageing experiments, and shows that at 350° C the $L1_2$ phase exists at a higher temperature than indicated by the extrapolated phase boundaries in the phase diagram of Raub *et al.* [12].

It was extremely difficult to determine the shape of the precipitates in Fig. 3 because of their small size, and examination of the diffraction patterns revealed rather unusual information. Diffraction patterns from thin foils oriented with zone axes [1 0 0], [1 1 0] and [1 1 1] are shown in Fig. 4. Diffuse superlattice reflections characteristic of the $L1_2$ crystal structure are visible in all three patterns, but those in the [1 0 0] pattern (Fig. 4a) are elongated along $\langle 1\,0\,0 \rangle$ whereas those in the other two are elongated parallel to $\langle 1\,1\,0 \rangle$. It is often the case that kinematical shape effects on electron diffraction spots are related to precipitate shapes when the particles are very small. However, we can think of no shape consistent with the effects observed in Fig. 4, and suspect that elastic strains might play an important role in the morphology of these precipitates.

3.2. Radiation damage

Three distinctive microstructural features were produced by the 400 keV proton irradiation, dislocations in various configurations, voids, and IIP. The experimental conditions over which each of these were

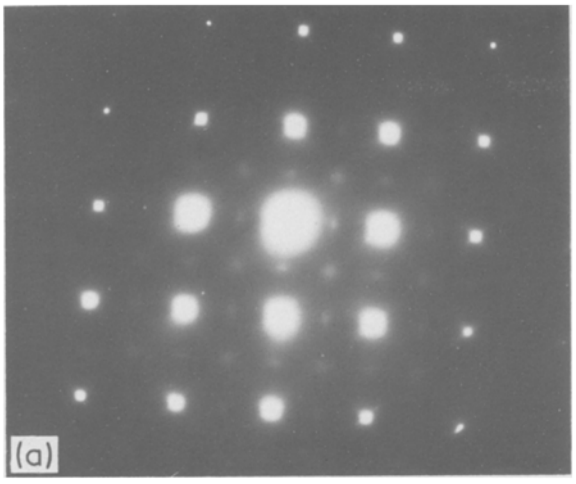

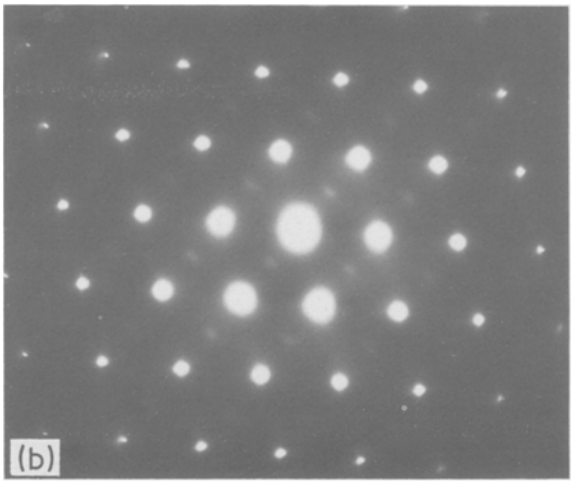

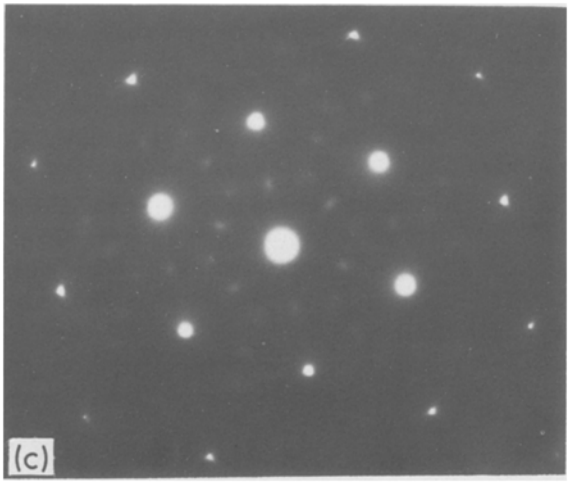

Figure 4 Illustrating the distortion of the superlattice reflections in the diffraction patterns of the unirradiated 25% Cr samples aged at 100° C. The zone axes in (a), (b) and (c) are [1 0 0], [1 1 0] and [1 1 1], respectively.

found are summarized in Table II and described individually in the following subsections.

3.2.1. Dislocation microstructures

The dislocation microstructures observed in proton-irradiated Pd–Cr alloys are quite complex and visually striking at the lower irradiation temperatures, as shown in Fig. 5. At T_{irr} = 350 and 450° C rafts of small dislocation loops lying on {1 1 1} are seen in all three alloys at a dose of 0.7 d.p.a., while at 100° C the loops are homogeneously distributed and at 550° C the dislocations configuration is network-like. Judging from the presence of streaks parallel to ⟨1 1 1⟩ in the electron diffraction patterns, the small loops observed at 100° C also lie on {1 1 1} and are faulted.

Other features of the dislocation microstructures are seen more clearly in Fig. 6. The individual loops in the raft configuration are visible in Fig. 6a (15% Cr, 350° C). In the 25% Cr sample, T_{irr} = 450° C, evidence is seen for an association between the dislocation loops and stacking faults. For example, a widely extended stacking fault ribbon is shown in Fig. 6b (at A), which appears to tail off into an array of individual loops. Fig. 6c shows a raft of loops, all of which appear to be faulted judging from the dark contrast within. In Fig. 6d there is evidence that the extended stacking-fault ribbon observed has a multiple-layer structure, indicating that secondary dislocation loops have nucleated and grown on a pre-existing fault. A TEM micrograph of a large area of a 25% Cr sample, T_{irr} = 450° C, is shown in Fig. 7. The microstructure observed illustrates the intimate association between the rafts of dislocation loops and stacking-fault ribbons on {1 1 1} in the Pd–Cr alloy system.

At T_{irr} > 500° C the dislocation density is smaller and the dislocation microstructure much less complex. The dominant feature is individual dislocation lines, which probably exist as part of a three-dimensional network which is not visible because it is truncated by the foil surfaces. Fig. 8 illustrates helical dislocations and dislocations pinned by voids in samples irradiated at 550° C. These features indicate that dislocation climb is a relatively easy process during irradiation at this temperature.

TABLE II Summary of irradiation-induced microstructural features observed in the Pd–Cr alloys*

Chromium (%)	Feature	Temperature (° C)						
		100	325	350	400	450	480	550
15	Dislocations	–	Y	Y	Y	Y	–	Y
	Voids	–	N	N	N	N	–	N
	IIP	–	N	N	N	N	–	N
20	Dislocations	Y	–	Y	–	Y	–	Y
	Voids	N	–	N	–	N	–	N
	IIP	N	–	Y	–	N	–	N
25	Dislocations	Y	–	Y	–	Y	Y	Y
	Voids	N	–	Y	–	Y	Y	Y
	IIP	Y†	–	Y†	–	Y	Y	Y

*Y = presence, N = absence, (–) condition not studied.
†Precipitation at these temperatures also results from isothermal ageing.

3.2.2. Voids

Voids were observed only in the 25% Cr samples at 350 ⩽ T_{irr} ⩽ 550° C. The voids were octahedral in shape, with faces parallel to {1 1 1}; examples are shown in Fig. 9. This shape was confirmed by examining the projected images of the voids along specific crystallographic directions. At T_{irr} = 550° C the shape was often irregular, the void surfaces not necessarily being confined to {1 1 1}. At T_{irr} = 450 and 480° C,

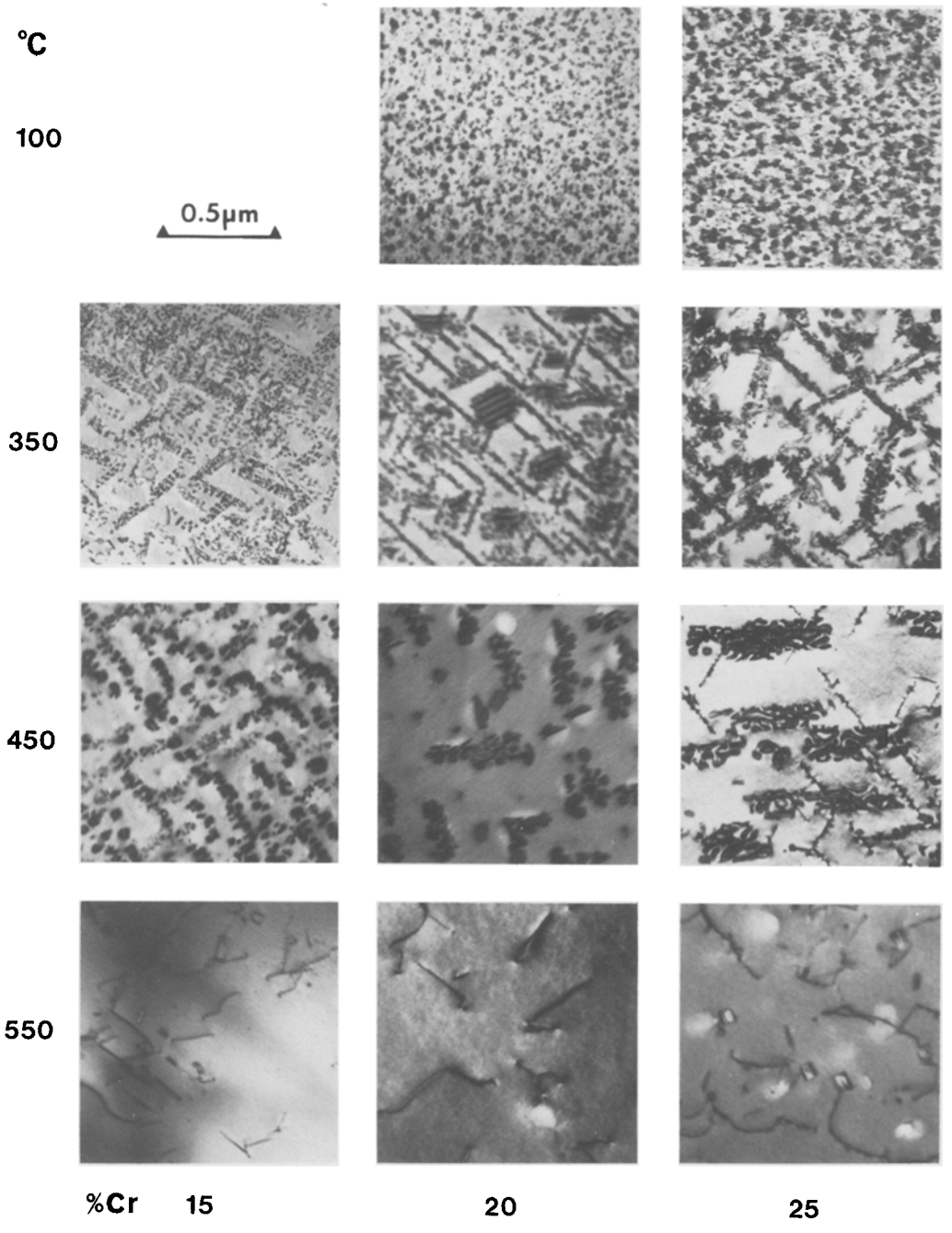

Figure 5 Typical dislocation microstructures observed in the Pd–Cr alloys irradiated to 0.7 d.p.a. with 400 keV protons at the temperatures indicated.

voids aligned in rows were sometimes seen; examples are shown in Fig. 10. Contrast experiments were performed to determine whether such strings of voids were associated with dislocation lines, but no convincing evidence was found to support this idea.

The edge length, d, of the octahedral voids (indicated in Fig. 9a) and concentration, N_v, were measured, producing the results presented in Table III. It is evident that d increases monotonically as T_{irr} increases, but that N_v passes through a maximum value at 480° C. Because of the behaviour of N_v, the volume fraction of voids (or equivalently the void swelling, $\Delta V/V = 2^{1/2}d^3N_v/6$) also passes through a maximum at 480° C. Behaviour similar to this was found in proton-irradiated Ni–Cr and Ni–Ti alloys by Pinizzotto *et al.* [17].

TABLE III Characteristics of the void microstructures observed at a depth of 1.2 μm from the surface in samples of the 25% Cr alloy

T (° C)	d (nm)	$N_v \times 10^{-11}$ (mm^{-3})	$\Delta V/V \times 10^3$
350	12.0	1.97	0.34
450	14.0	8.85	2.43
480	17.5	11.60	6.22
550	30.0	1.39	3.75

3.2.3. Precipitation during irradiation

The conditions under which precipitation of the $L1_2$ phase was observed are summarized in Table IV. From the results of the ageing experiments it is obvious that precipitation was truly *induced* by proton irradiation in the 20% Cr samples and in the 25% Cr samples at $T_{irr} > 350$° C; in all other instances the precipitation of the $L1_2$ phase was enhanced or accelerated by irradiation rather than induced. An example

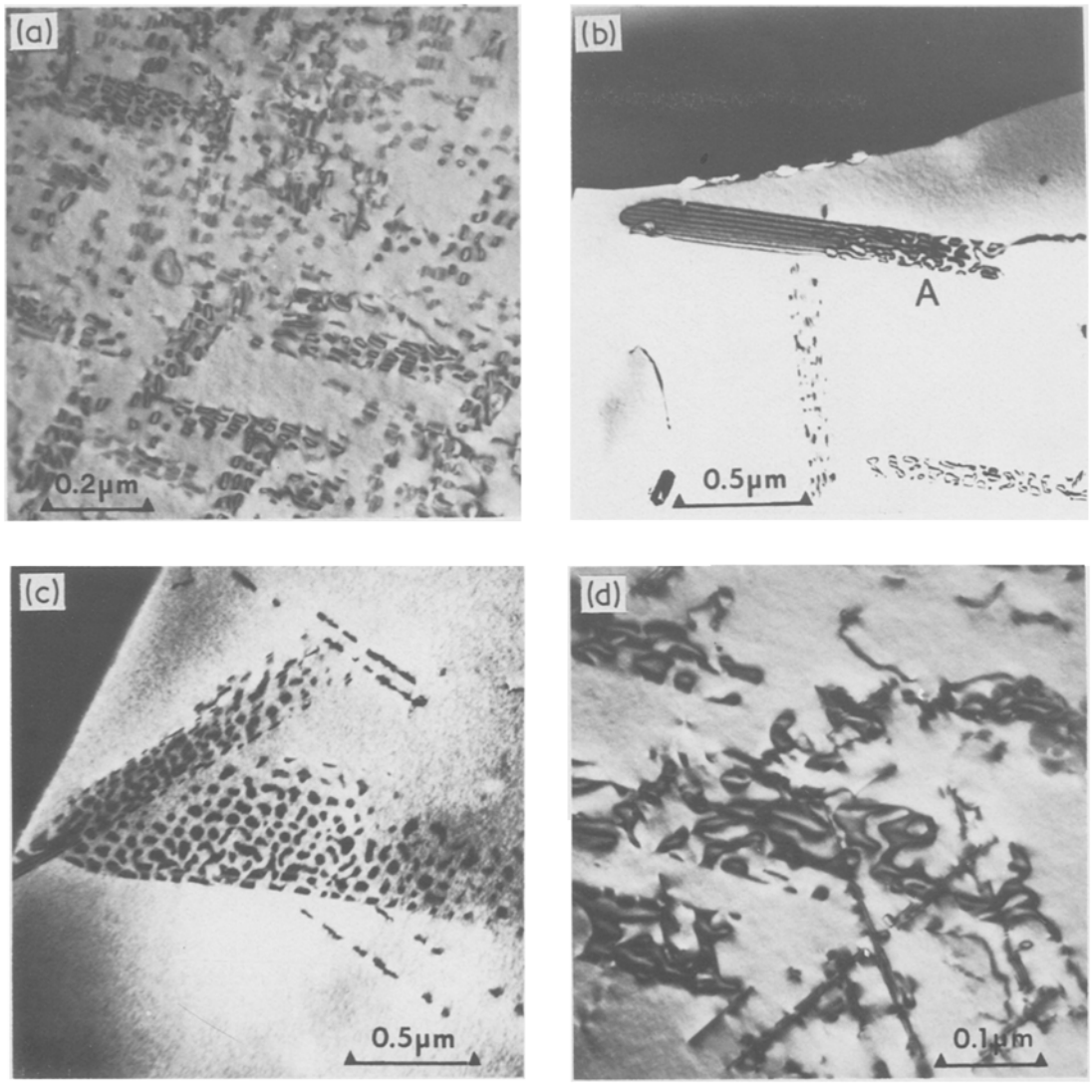

Figure 6 Dislocation configurations observed in samples of (a) 15% Cr alloy irradiated to 0.68 d.p.a. at 350° C; (b) to (d) 25% Cr alloy irradiated to 0.70 d.p.a. at 450° C. In (b) a seemingly perfect stacking-fault ribbon (at A) appears to have broken up into, or to have been consolidated from individual faulted dislocation loops.

of irradiation-enhanced precipitation at 100° C is shown in Fig. 11. Black dot contrast, probably arising from small dislocation loops, is present in the 25% Cr alloy after 3 h of irradiation (Fig. 11a), and it is difficult to determine whether there is a correspondence between them and the finely dispersed precipitates seen in Fig. 11b. The precipitates in this sample are significantly larger than those in the sample of the same alloy aged for 7 days at 100° C (cf. Fig. 3a).

The precipitate morphology in the 25% Cr sample irradiated at 350° C is completely different from that in Figs 3b and 11. The precipitates observed in the dark-field image (Fig. 12b) are definitely associated with the rafted dislocation loops seen in Fig. 12a. The role of solute segregation in the irradiation-enhanced precipitation of the $L1_2$ phase is clearly significant at the higher T_{irr}. Unlike the case of the samples unirradiated but aged at 350° C, the diffraction patterns show evidence of streaking only along ⟨1 1 1⟩ (Fig. 12c), underscoring the morphological differences of the precipitates that form during conventional ageing (cf. Fig. 4) and under irradiation.

TABLE IV Spatial distribution of IIP and its occurrence at various point-defect sinks in Pd–Cr alloys*

Position	20% Cr, 350° C	25% Cr				
		100° C	350° C	450° C	480° C	550° C
Surface	N	Y	Y	Y	Y	N
Mid-range	Y	Y	Y	Y	Y	Y
Dislocations	Y	Y	Y	Y	Y	Y
Voids	N	N	Y	Y	Y	Y
Grain boundaries	N	N	N	Y	Y	N

*Y = presence, N = absence of IIP.

True IIP occurred in the 20% Cr samples at T_{irr} = 350° C and in the 25% Cr samples at T_{irr} > 350° C (Table IV). Clear evidence of the strain fields produced by solute segregation to dislocation loops are seen in Fig. 13. The strain fields, most readily visible at the loops viewed edge-on in the foil, are due to the migration of chromium to the loops and the precipitation of the $L1_2$ phase on the loops themselves. The strain is caused by the difference between the lattice parameters of the palladium solid solution and the $L1_2$ phase. Since a precise determination of the lattice constant of the $L1_2$ phase has not been made, we estimated it by comparing the interplanar spacings of the reflections of the fcc and precipitate phases in

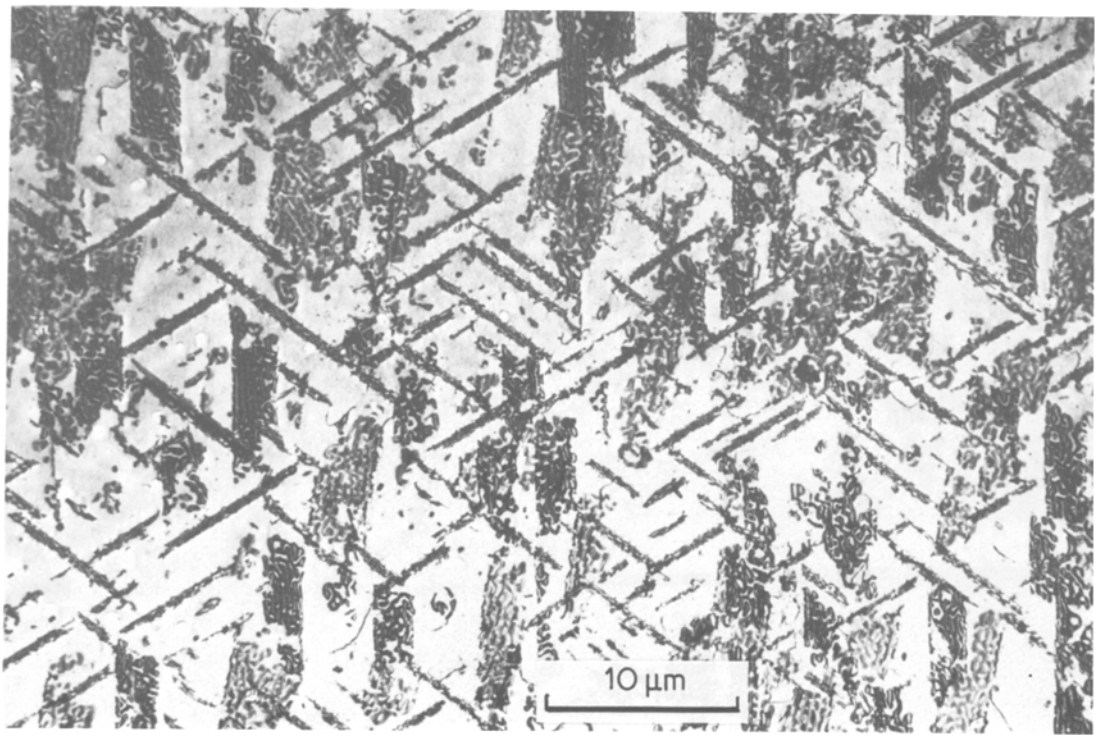

Figure 7 Illustrating the characteristic morphology of the stacking faults in the 25% Cr alloy irradiated at 450° C to 0.7 d.p.a.

the 25% Cr sample irradiated at 450° C. The lattice constant of the $L1_2$ phase was estimated to be 0.37955 nm, measured relative to that of the 25% Cr solid solution, 0.38620 nm [18, 19], producing a lattice misfit calculated to be approximately −1.72%.

Fig. 14 illustrates IIP typically seen at dislocations, stacking faults and voids, and Fig. 15 shows examples of IIP at grain boundaries, with their adjacent precipitate-free zones. These features are very similar to those seen in proton-irradiated Ni–Si alloys.

According to the phase diagram (Fig. 1), solute enrichment in the 25% Cr alloy irradiated at 550° C could produce IIP of an ordered phase with the $L1_0$ crystal structure (PdCr) provided that solute segregation drives the local concentration to a level of ~35% Cr. Convincing evidence for the IIP of this phase was not obtained. Very weak superlattice reflections were observed in the diffraction patterns, and a limited amount of IIP on dislocations and voids was found, as shown in Fig. 16. According to Raub and Mahler [19] PdCr is fct with lattice constants $a = 0.3869$ and $c = 0.3792$ nm (cf. $a = 0.3796$ nm for the $L1_2$ phase, as estimated by us). Owing to the small differences among these values and the diffuseness of the superlattice reflections in Fig. 16c, a positive determination of the crystal structure of the precipitates seen in Figs 16a and b could not be made.

The foregoing results were obtained on thin foils taken from the mid-range region of the irradiated samples, typically at distances between 1.0 and 1.5 μm from the surface. Samples from other regions of the damage profile (Fig. 2) were examined, however, as indicated in Table IV. IIP was seen in the surface

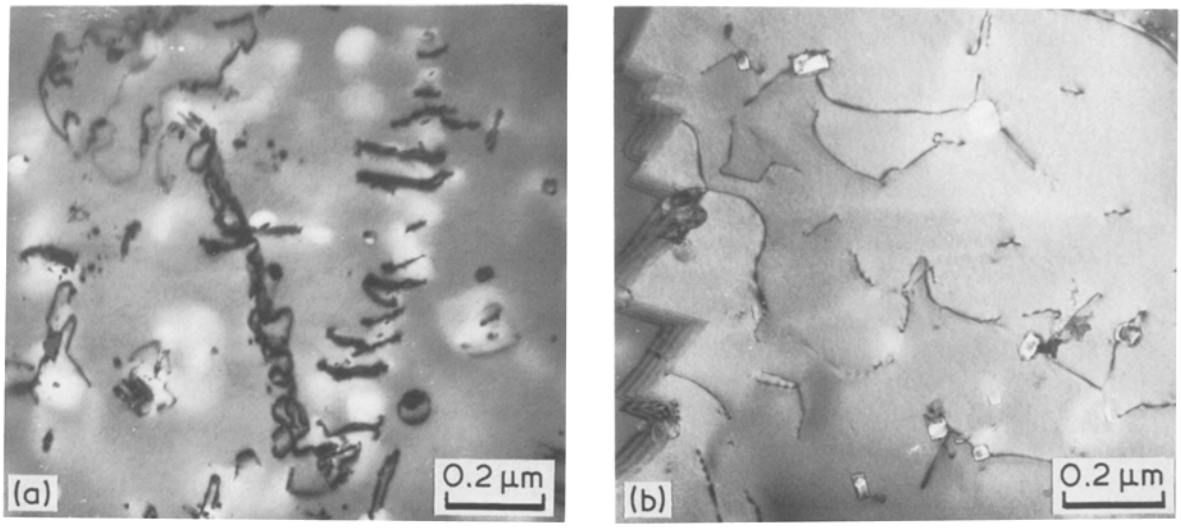

Figure 8 Illustrating (a) helical dislocations and (b) dislocations pinned at voids in the 25% Cr alloy irradiated to 0.63 d.p.a. at 550° C.

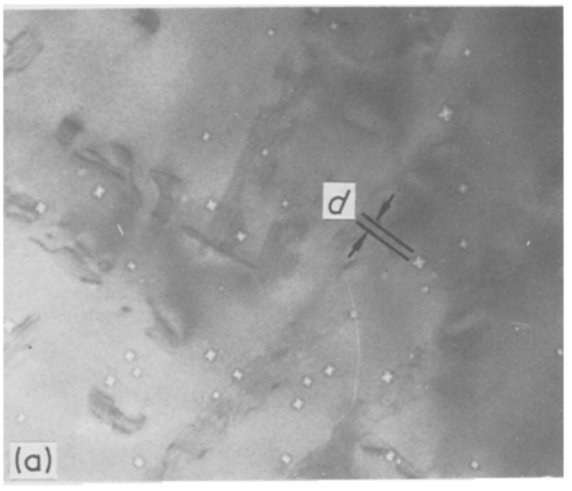

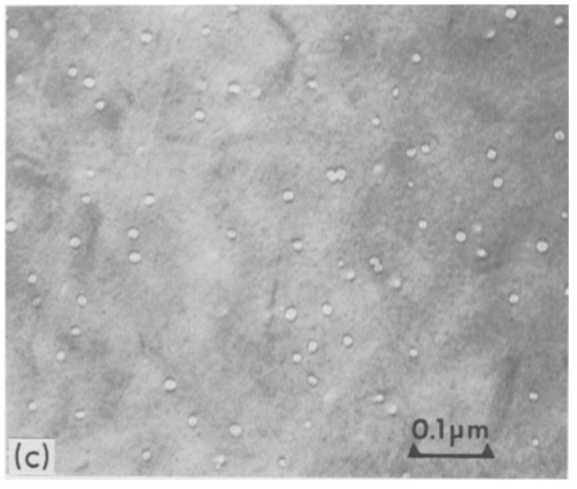

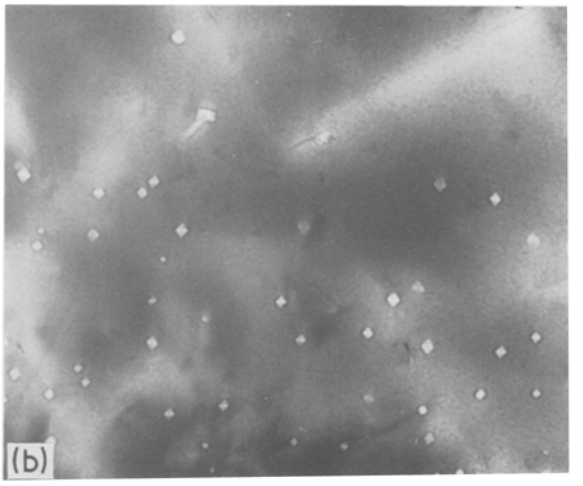

Figure 9 The void morphology in the 25% Cr samples observed with the electron beam parallel to (a) [1 0 0]; (b) [1 1 0]; (c) [1 1 1]. The edge length, d, of the octahedrally shaped voids is indicated in (a).

regions (these thin foils were prepared simply by back-polishing the irradiated samples), but samples taken from the region between 0.2 and 1.0 μm and beyond 1.5 μm contained dislocations or voids, with no evidence of IIP.

The conventional experiment that enables IIP to be distinguished from irradiation-enhanced precipitation is post-irradiation annealing, preferably at T_{irr}. Such experiments were performed on all the samples in which IIP was observed. The precipitates in the 20% Cr sample (T_{irr} = 350° C) and the 25% Cr sample irradiated at 550° C dissolved after 72 h, while 20 days at 480° C were required to dissolve the precipitates in the 25% Cr sample. The sample irradiated at 450° C contained precipitates even after ageing for 20 days at this temperature. There is little doubt, then, that precipitation in three out of these four conditions is induced. The result on the 25% Cr sample at T_{irr} = 450° C, combined with ageing of the unirradiated alloy at this temperature, suggests that 450° C is close to the solubility limit, somewhat contradicting the results portrayed in Fig. 1. Nevertheless, because of the proximity to the solubility limit, the driving force for dissolution of IIP (or normal precipitation during ageing) is expected to be small, and it is possible that the precipitates in this sample would have dissolved had the post-irradiation ageing treatment at 450° C been continued beyond 20 days.

The dislocation microstructure during post-irradiation annealing changes from the orderly arrays of dislocation loops to randomly curved dislocation lines. The dislocation density decreases with increasing ageing time, as seen in Fig. 17. Fig. 18a, which is the dark-field image corresponding to Fig. 17b, shows that the precipitates of the $L1_2$ phase also change shape and appear to grow. This most likely happens because 480° C is close to the solubility limit so that coarsening competes with dissolution during the initial stage of post-irradiation ageing, producing temporary precipitate growth prior to eventual disappearance. Voids persist even in the samples aged for 20 days, and some of them coalesce to form much larger voids, with a void-depleted zone nearby (Fig. 18b).

4. Discussion

The microstructures observed in proton-irradiated Pd–Cr alloys are similar in many respects to those seen in Pd–Fe and Ni–Si alloys irradiated under comparable conditions, but it is the differences that are particularly interesting. The most noteworthy differences are that rafting of dislocation loops is seen

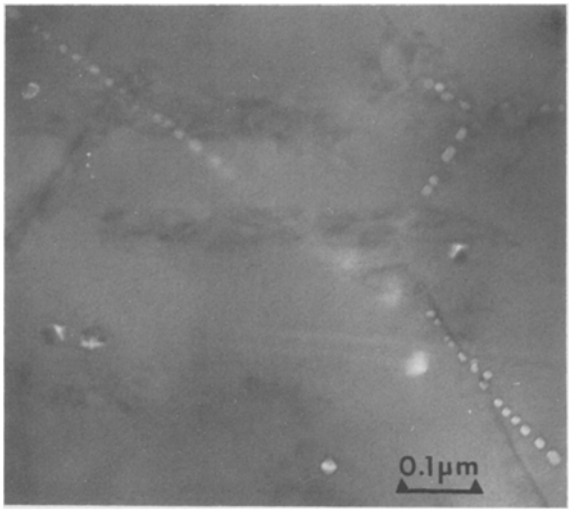

Figure 10 Aligned voids seen in the 25% Cr alloy irradiated to 0.70 d.p.a. at 450° C.

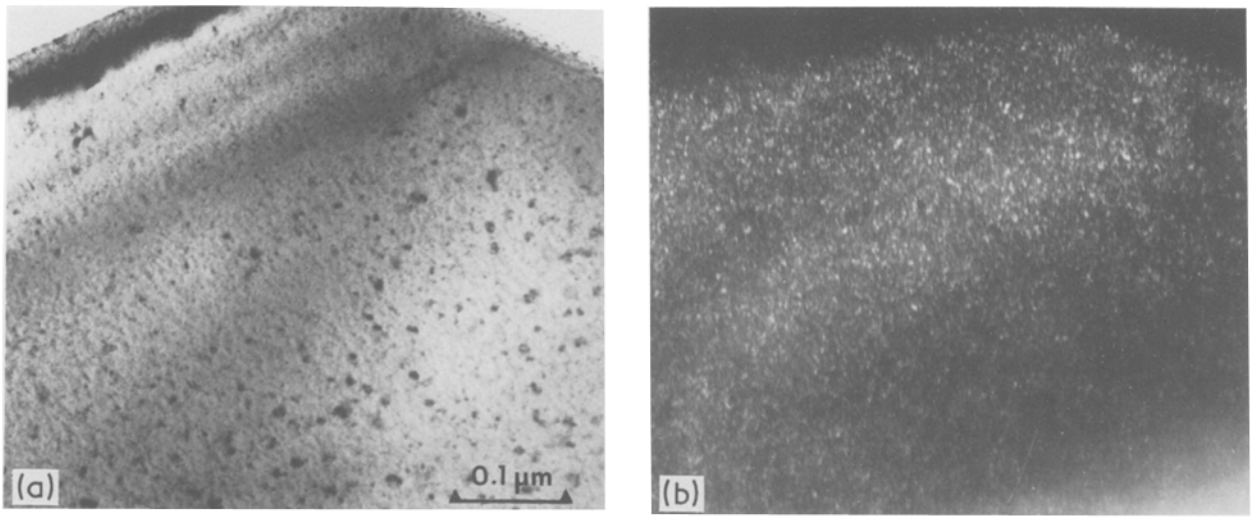

Figure 11 Illustrating the radiation damage in the 25% Cr alloy irradiated at 100° C to a dose of 0.70 d.p.a.: (a) bright-field image; (b) dark-field image of the same area as (a), taken using a superlattice reflection from the $L1_2$ phase.

only in Pd–Cr alloys and that voids in this system are found only in the most concentrated alloy, whereas voids are produced in the other alloys at all the concentrations examined. Unlike the Ni–Si system, in which IIP occurs even in dilute alloys, IIP in Pd–Cr and Pd–Fe alloys is observed only when the solute concentration is large.

There appears to be no ready explanation for the rafting phenomenon; to the best of our knowledge it is unique to irradiated Pd–Cr alloys. It may be related to the effect of chromium on the stacking-fault energy, which appears to be low although its magnitude in palladium alloys in general is unknown. Alternatively the elastic anisotropy of palladium may be such that the presence of a dislocation loop that has already nucleated stimulates the nucleation of a neighbouring loop on the same $\{1\,1\,1\}$ plane, so that the nucleation process is not random. This would appear to be the more likely alternative, but in the absence of calculations of elastic interactions confirmation of this suggestion is not possible.

The observation of void formation at only one value of the chromium concentration is likewise mysterious. Explanations have been proposed for the minima in void swelling found in the Ni–Cr and Ni–Ti systems [17], but the swelling behaviour in these alloys, as well as the aforementioned Ni–Si and Pd–Fe systems, varies continuously with solute concentration.

IIP in Pd–Cr and Pd–Fe alloys is quite similar in that it is found only in concentrated alloys. It differs from that in Ni–Si alloys in that surface films of the $L1_2$ phase are never observed, nor is the induced homogeneous precipitation (IIHP) of this phase ever observed. The absence of IIHP is partly due to the slower variation of S_D with distance from the surface in the peak damage region, which is much more sharply peaked in nickel [6]. This produces a smaller flow or point defects into the mid-range region of the damage production curve, as discussed by Janghorban

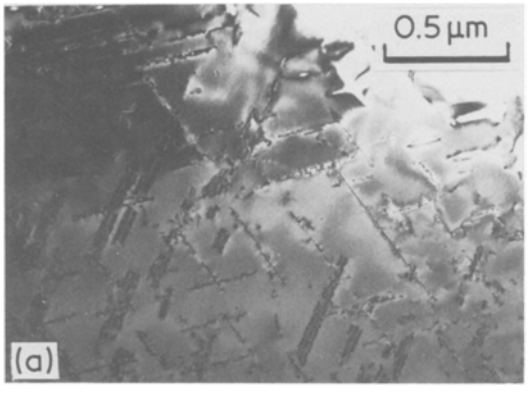

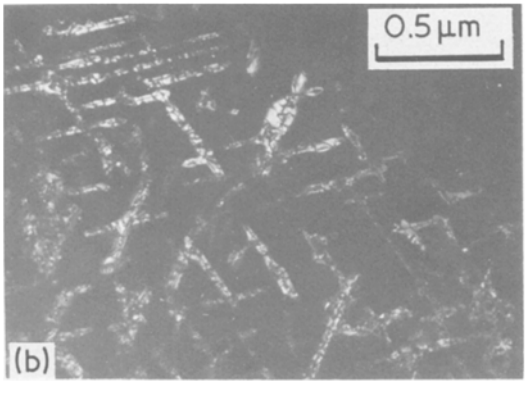

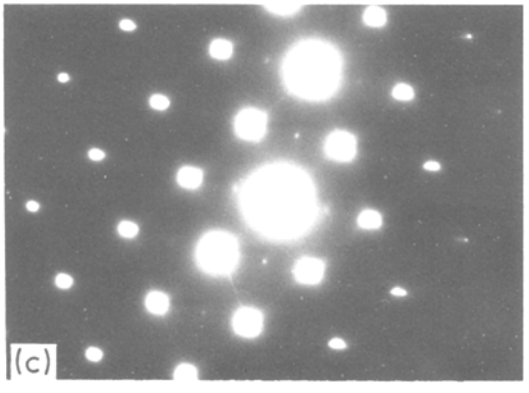

Figure 12 Precipitate morphology seen in the 25% Cr alloy irradiated at 350° C to a dose of 0.78 d.p.a.: (a) bright-field image; (b) dark-field image of the same area as (a), taken using a superlattice reflection from the $L1_2$ phase; (c) diffraction pattern from (a) and (b) illustrating the streaks parallel to $\langle 1\,1\,1 \rangle$.

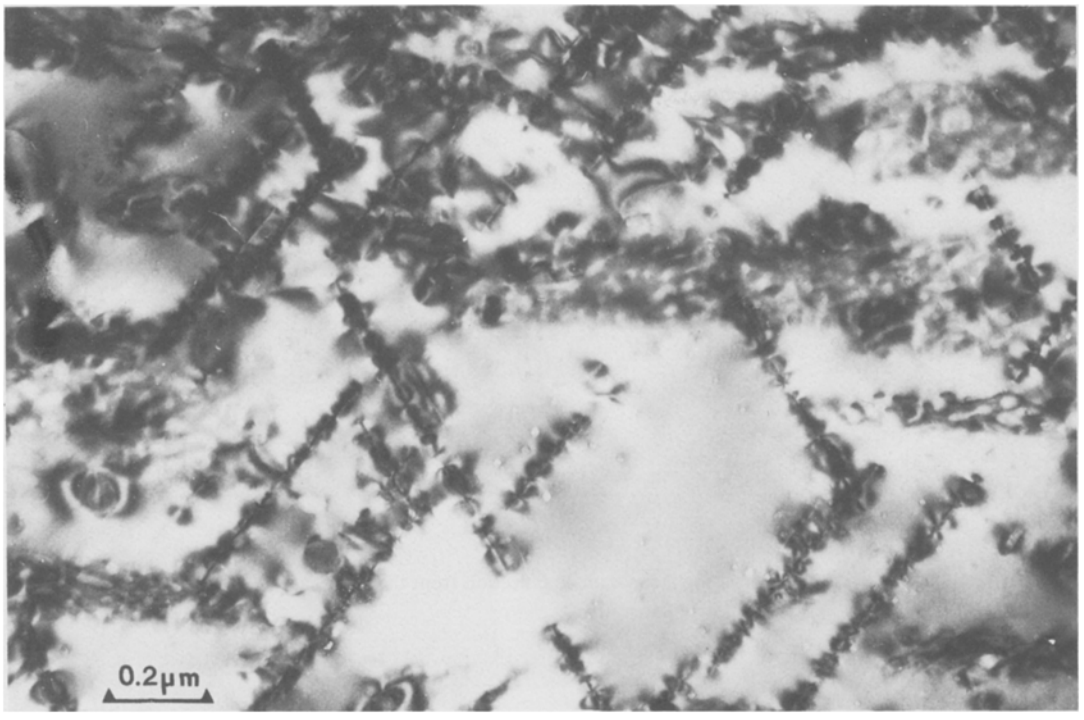

Figure 13 Illustrating the strain fields associated with dislocations (or stacking faults) on which IIP has occurred in the 25% Cr samples irradiated to 0.7 d.p.a. at 450° C.

and Ardell [6] and Lam *et al.* [20]. However, the interstitial-solute atom coupling in Pd–Cr alloys must also be significantly smaller than in Ni–Si alloys, consistent with the behaviour of Pd–Fe alloys, as suggested by Janghorban and Ardell [6], otherwise surface films of the $L1_2$ phase would be expected to form. Furthermore, the mobility of vacancies in Pd–Cr alloys seems to be as anomalously high as in Pd–Fe alloys, which is the only logical explanation for the precipitation of the $L1_2$ phase during isothermal ageing of unirradiated samples of the 25% Cr alloy at 100° C. The high vacancy mobility promotes back-diffusion of the solute atoms, thereby further reducing the tendency towards IIHP and the formation of surface films of the $L1_2$ phase.

The results on IIP of the $L1_2$ phase in this study substantiate the conclusion reached by Janghorban and Ardell [6] in their work on Pd–Fe alloys that a negative value of η may be necessary for the occurrence of IIP, but is not sufficient. Strong interstitial-solute atom binding is also required to drive solute segregation to the point that the solubility limit is reached at point-defect sinks, and solute diffusion by vacancies must be slow enough that the concentration gradients created by solute segregation are not reduced to insignificant levels by back-diffusion.

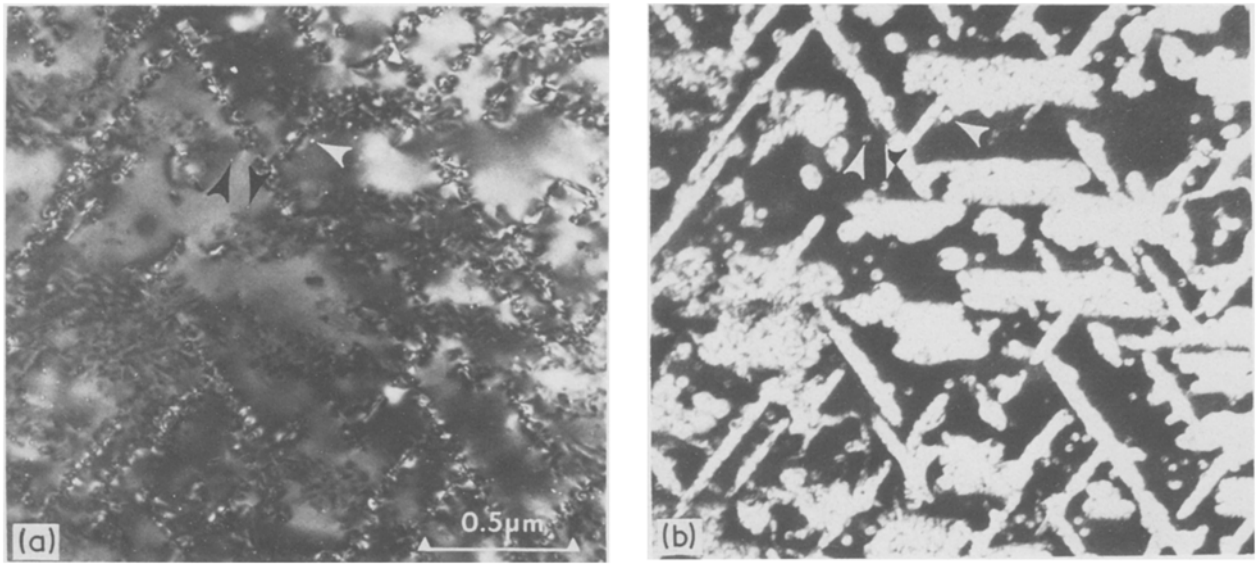

Figure 14 Illustrating the evidence for the occurrence of IIP at voids in the 25% Cr alloy irradiated at 450° C to a dose of 0.7 d.p.a. The small voids indicated by the arrows in the bright-field image (a) appear bright in the dark-field image (b), taken using a superlattice reflection from the $L1_2$ phase.

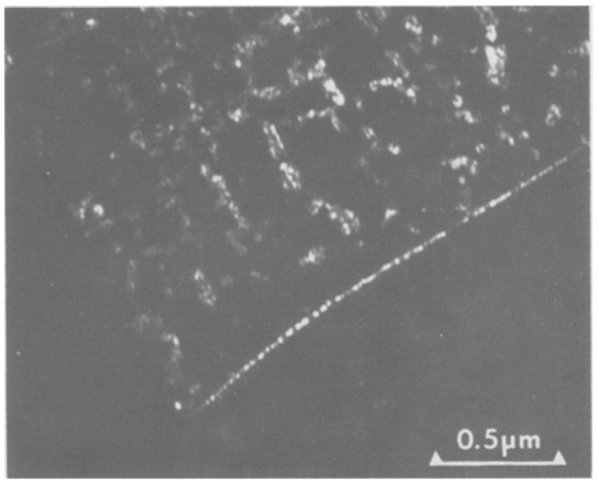

Figure 15 IIP on grain boundaries in the 25% Cr alloy irradiated to 0.63 d.p.a. at 480° C.

5. Summary and conclusions

1. Precipitation of the $L1_2$ phase occurs in unirradiated samples of the 25% Cr alloy aged at 100 and 350° C. These very low ageing temperatures suggest that vacancy diffusion is quite rapid, probably anomalously so, in this alloy. Precipitation in the 25% Cr alloy is accelerated by irradiation at 100 and 350° C. It is clearly heterogeneous at the higher temperature, but at 100° C the dislocation loops are too small to

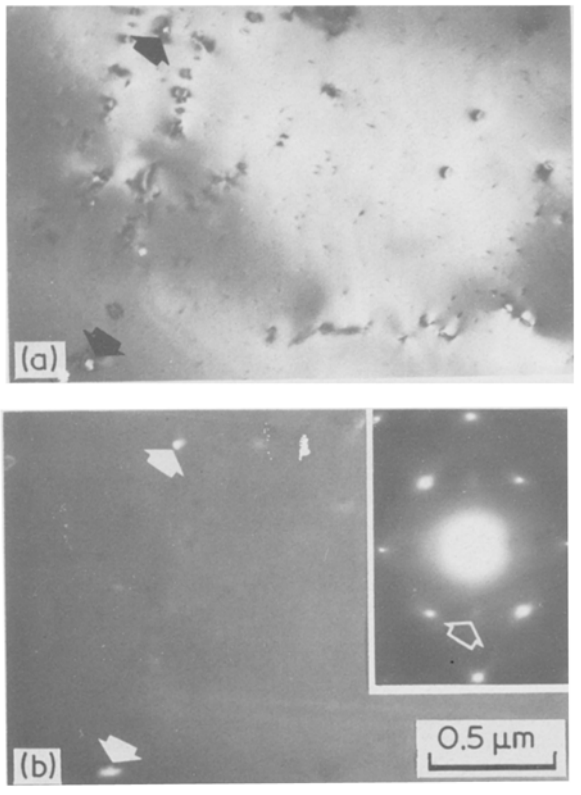

Figure 16 (a) Bright-field and (b) dark-field electron micrographs of the same area suggesting the occurrence of IIP on voids in the 25% Cr alloy irradiated to 0.63 d.p.a. at 550° C. The dark-field image was taken using the reflection indicated by the arrow in the diffraction pattern inset in (b).

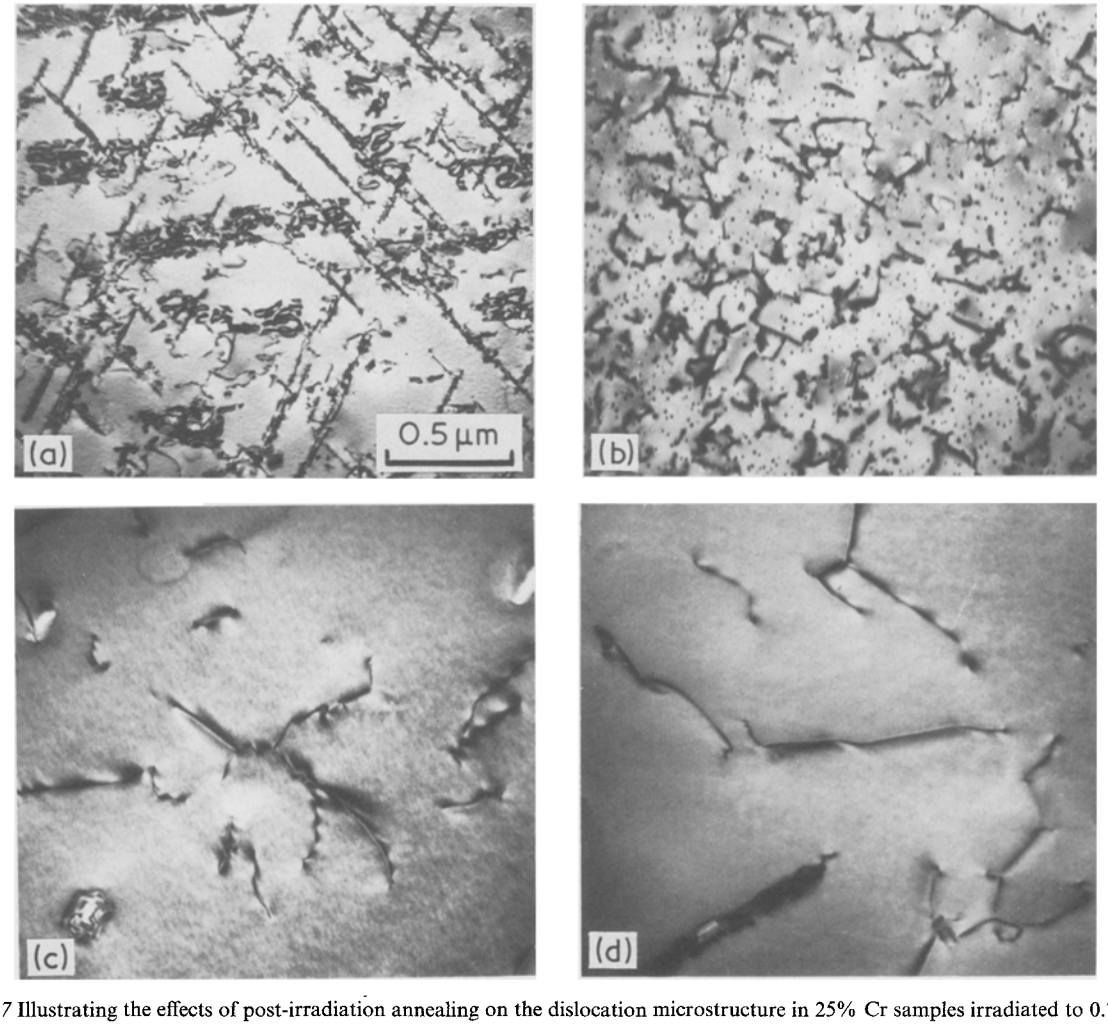

Figure 17 Illustrating the effects of post-irradiation annealing on the dislocation microstructure in 25% Cr samples irradiated to 0.77 d.p.a. at 480° C: (a) as-irradiated; (b) after ageing at 480° C for 3 days; (c) after 12 days; (d) after 20 days.

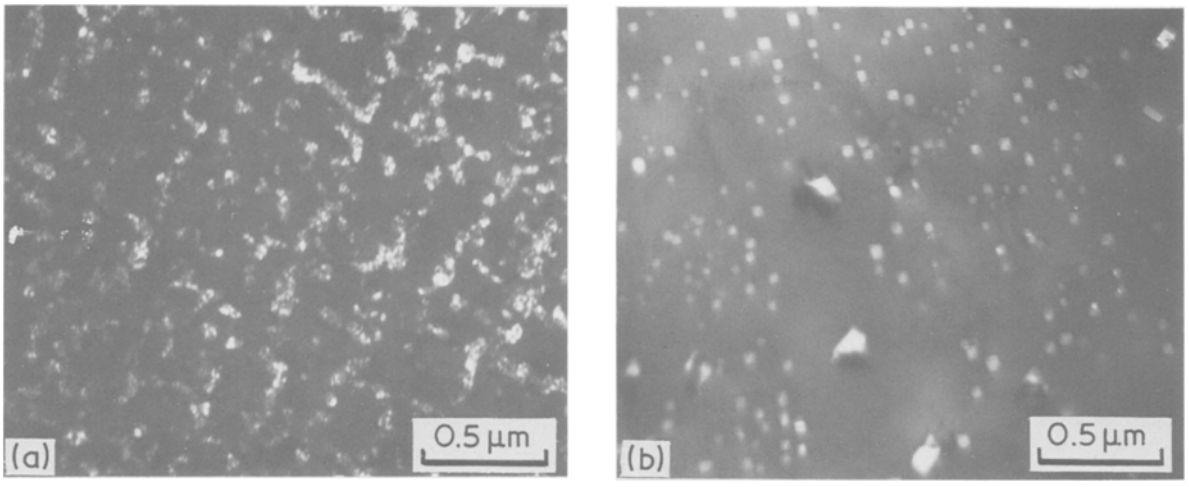

Figure 18 (a) Dark-field image of the area in Fig. 17b taken using a superlattice reflection from the $L1_2$ phase; (b) voids observed in the 25% Cr sample irradiated to 0.77 d.p.a. at 480° C and then aged at this temperature for 20 days.

determine a definitive correspondence with the precipitates observed.

2. A unique feature of the dislocation loops produced during irradiation is the pronounced tendency towards rafting along {1 1 1} in all three alloys irradiated at 350 and 450° C. The mechanism of this phenomenon is unknown, although elastic interactions among the loops and a low stacking-fault energy are most likely involved.

3. Voids are observed only in the 25% Cr alloy. Their average size increases monotonically with increasing T_{irr} in the range 350 to 550° C, but N_v passes through a maximum at 480° C. Maximum swelling also occurs at this temperature.

4. The undersized chromium atoms ($\eta = -0.0250$) segregate towards all the familiar point-defect sinks. When IISS drives the local chromium concentration to a level exceeding the solubility limit IIP occurs, except at the free surface of the samples. It has been observed at dislocation loops, voids, stacking faults and grain boundaries, but only in the 20% Cr alloy at 350° C and in the 25% Cr alloy at $T_{irr} > 350$° C; it was not found in the 15% Cr alloy under any irradiation condition.

5. Whenever IIP occurs it does so in the mid-range region of the samples. It appears in the near-surface region only in the 25% Cr alloy irradiated at 450 and 480° C. This is attributed to the strong segregation in the mid-range region brought about by the steep gradient in the damage production profile.

6. IISS and IIP in proton-irradiated Pd–Cr and Pd–Fe alloys are very similar, but quite different from IISS and IIP in Ni–Si alloys in which the solute segregation effect is much stronger. Since the values of η in all three alloys are comparable, it is concluded that the smaller effect in the palladium-base alloys is due to weaker interstitial-solute atom coupling combined with a high vacancy mobility. The high mobility promotes rapid back-diffusion which reduces the concentration gradients induced by solute segregation. It is also consistent with the low-temperature precipitation of the $L1_2$ phase observed in unirradiated samples.

Acknowledgements

The authors are grateful to the Department of Energy, Office of Basic Energy Sciences, Division of Materials Sciences, for their financial support of this research. O. Ajaja would also like to thank the International Atomic Energy Authority for its assistance in the form of an IAEA Fellowship.

References

1. P. R. OKAMOTO, A. TAYLOR and H. WIEDERSICH, in "Fundamental Aspects of Radiation Damage in Metals", Vol. 2, edited by M. T. Robinson and F. W. Young Jr (CONF-751006-P2, 1975) (National Technical Information Service, US Dept. of Commerce, Springfield, VA22161) pp. 1188–1195.
2. A. BARBU and A. J. ARDELL, *Scripta Metall.* **9** (1975) 1233.
3. G. SILVESTRE, A. SILVENT, C. REGNARD and G. SAINFORT, *J. Nucl. Mater.* **57** (1975) 125.
4. K. JANGHORBAN and A. J. ARDELL, *ibid.* **85/86** (1979) 719.
5. A. BARBU, "Irradiation Behaviour of Metallic Materials for Fast Reactor Core Components", edited by J. P. Poirier (CEA, Gif sur Yvette, France, 1979) pp. 67–73.
6. K. JANGHORBAN and A. J. ARDELL, *J. Nucl. Mater.* **114** (1983) 66.
7. L. WEAVER and A. J. ARDELL, *Scripta Metall.* **14** (1980) 765.
8. *Idem,* in "Effects of Radiation on Materials: Tenth Conference, ASTM STP 725", edited by D. Kramer, H. R. Brager and J. S. Perrin (American Society for Testing and Materials, Philadelphia, 1981) pp. 610–626.
9. M. S. MOSTAFA and A. J. ARDELL, to be published.
10. A. J. ARDELL and K. JANGHORBAN, in "Phase Transformations During Irradiation", edited by F. V. Nolfi Jr (Applied Science, New York, 1983) pp. 291–329.
11. *Idem,* in "Thermodynamics and Kinetics of Metallurgical Processes (ICMS-81)", edited by M. Mohan Rao, K. P. Abraham, G. N. K. Iyengar and R. M. Mallya (Indian Institute of Metals, Calcutta, 1985) pp. 259–285.
12. V. E. RAUB, R. GOHLE and E. ROSCHEL, *Z. Metallkde* **58** (1967) 567.
13. R. F. PINIZZOTTO Jr, PhD dissertation, University of California (1978).
14. H. R. BRAGER, H. E. KISSINGER and G. L. KULCINSKI, *Radiat. Eff.* **5** (1970) 281.
15. J. P. BIERSACK and L. G. HAGGMARK, *Nucl. Instr. Meth.* **174** (1980) 257.

16. T. D. RYAN, PhD dissertation, University of Michigan (1975).
17. R. F. PINIZZOTTO Jr, L. J. CHEN and A. J. ARDELL, *Metall. Trans. A* **9A** (1978) 1718.
18. G. GRUBE and R. KNABE, *Z. Elektrochem.* **42** (1936) 793.
19. E. RAUB and W. MAHLER, *Z. Metallkde* **45** (1954) 648.
20. N. Q. LAM, K. JANGHORBAN and A. J. ARDELL, *J. Nucl. Mater.* **101** (1981) 2.

Received 3 March
and accepted 28 April 1987